

# Adaptive optics system for the IRSOL solar observatory

Renzo Ramelli<sup>a</sup>, Roberto Bucher<sup>b</sup>, Leopoldo Rossini<sup>a,b,c</sup>, Michele Bianda<sup>a</sup>, Silvano Balemi<sup>b</sup>

<sup>a</sup>Istituto Ricerche Solari Locarno, Via Patocchi, Locarno, Switzerland;

<sup>b</sup>Scuola Universitaria Professionale della Svizzera Italiana, Le Gerre, Manno, Switzerland;

<sup>c</sup>Swiss Center for Electronics and Microtechnology, Jaquet-Droz 1, Neuchâtel, Switzerland

## ABSTRACT

We present a low cost adaptive optics system developed for the solar observatory at Istituto Ricerche Solari Locarno (IRSOL), Switzerland. The Shack-Hartmann Wavefront Sensor is based on a Dalsa CCD camera with 256 pixels x 256 pixels working at 1kHz. The wavefront compensation is obtained by a deformable mirror with 37 actuators and a Tip-Tilt mirror. A real time control software has been developed on a RTAI-Linux PC. Scicos/Scilab based software has been realized for an online analysis of the system behavior. The software is completely open source.

**Keywords:** Instrumentation, Adaptive Optics, Sun, IRSOL

## 1. INTRODUCTION

The solar observatory at Istituto Ricerche Solari Locarno (IRSOL) focuses its activity on precise spectropolarimetric measurements<sup>1</sup> from the near UV to the near infrared with its Gregory-Coudé telescope, which has a 45 cm aperture. The key-instrument is the Zurich Imaging Polarimeter (ZIMPOL)<sup>2,3</sup> that reaches a polarimetric sensitivity of  $10^{-5}$  thanks to fast (kHz) polarization modulation/demodulation of the light beam in combination with a special masked CCD. With this precision, it has been possible to explore in great detail the spectral dependence of the faint signatures of scattering polarization, which can be observed mainly near the solar limb. Since the scattering polarization signatures in the spectral lines are modified by the presence of a magnetic field through the Hanle effect,<sup>4</sup> it has been possible to access to new diagnostic capabilities on the solar magnetism.<sup>5</sup> The Hanle effect signatures give the possibility to obtain information on the magnetic fields, that are tangled below the resolution limit, and to which the Zeeman effect based diagnostics is blind due to cancellation effects.<sup>6</sup>

Even if the observing programs at IRSOL are focused on high polarimetric sensitivity rather than on obtaining diffraction limited high spatial resolution images, it is a clear advantage to install an AO system that allows reaching a good image stability during a long exposure measurement. A typical precise ZIMPOL observation last for few tens of minutes and combines thousands of frames with about 1 second exposure time each. Thus it has been decided to install a low cost adaptive optics system based on the concept and design of the adaptive optics (AO) system developed by Keller et al. (2003)<sup>7</sup> for the infrared at the McMath-Pierce solar telescope.

## 2. THE OPTICAL SETUP

A simplified scheme, showing the inclusion of the AO system in the global optical setups with the spectrograph or with the Fabry Perot filter system, is reported in Fig. 1. Most of the observations at IRSOL are obtained with the high dispersion Czerny-Turner spectrograph. Since a few years ago, a Fabry Perot filter system<sup>8,9</sup> based on two LiNbO<sub>3</sub> etalons is also available for observations in 2D imaging mode. The Fabry Perot system can also be used in a novel configuration in combination with the spectrograph.<sup>10</sup>

A picture of the optical bench with the AO system is shown on Fig. 2. The Tip-tilt mirror (TT) made by Piezosystem Jena works with three piezoactuators PSH8. The deformable mirror (DM) by Okotech with 15 mm diameter operates with 37 actuators. The folding mirror (FM1) and the dichroic beam splitter plate (BS) form a block that can be simply removed if one wants to observe without AO. The spherical mirrors (SM1 and SM2) form a telecentric system so that the optical characteristics of the light beam are the same with or without AO. Between FM and SM1 there is a focal plane where a pinhole is inserted during calibrations. The TT is re-imaged on the spectrograph grating so that tip-tilt corrections do not move the beam on the grating. The image of the

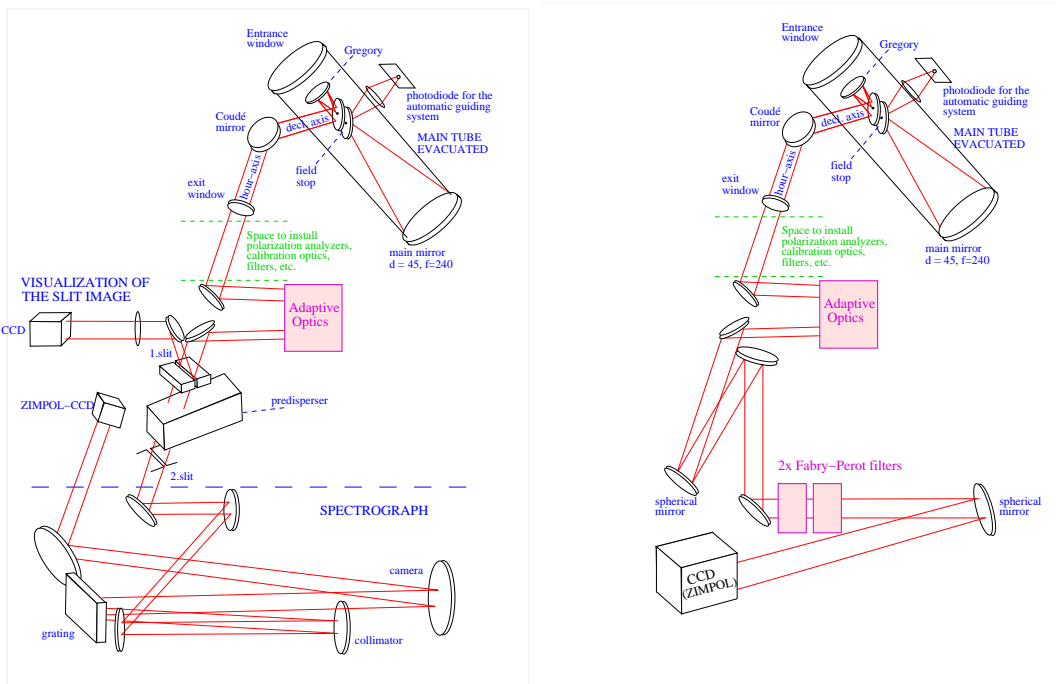


Figure 1. Simplified scheme (not to scale) of the optical setups at the telescope. On the left the setup with the spectrograph. On the right the setup with the Fabry Perot filter system

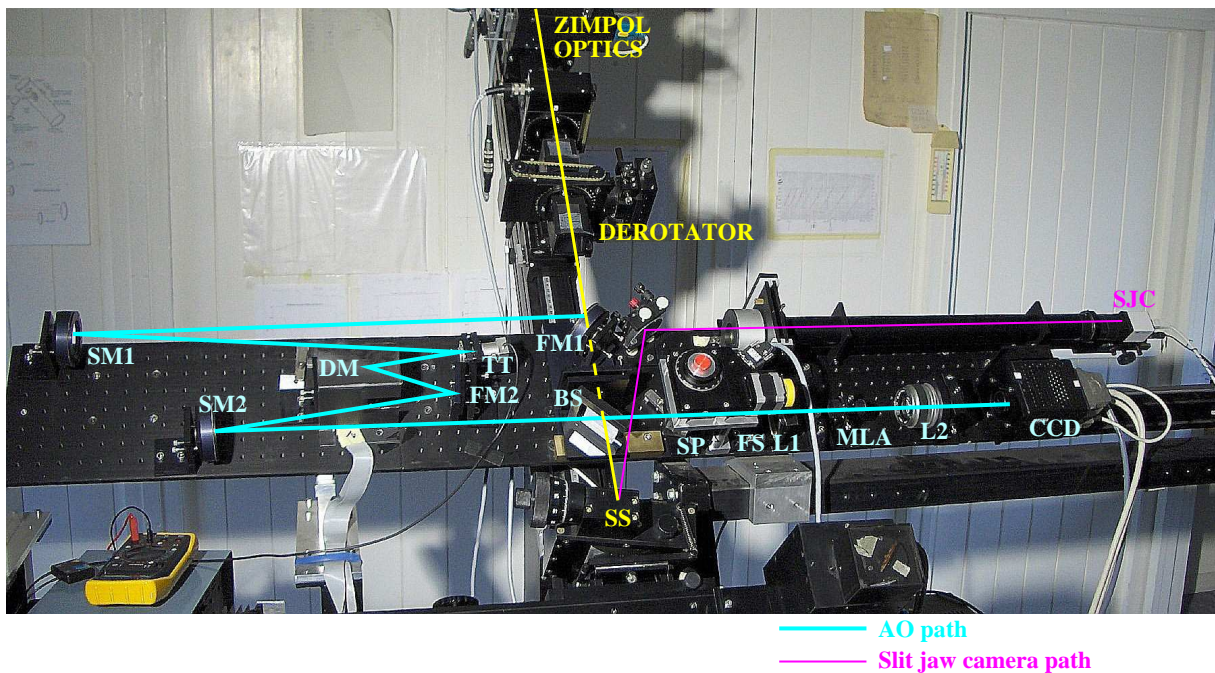


Figure 2. The optical bench with the AO system. (For details see text).

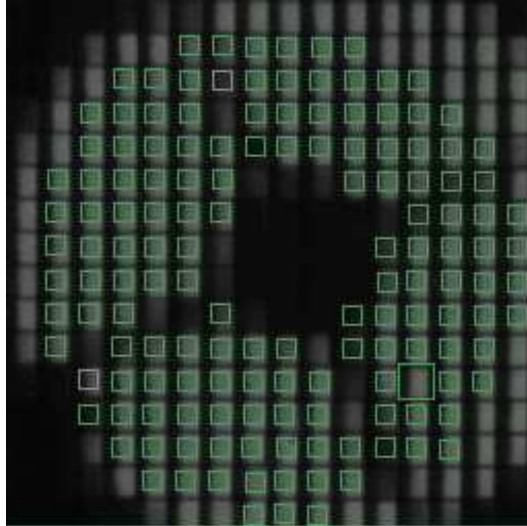


Figure 3. Image seen by the SH-WFS camera during limb tracking. The small squares represent the  $8 \times 8$  pixels sub-aperture images used for the wave front measurement. The large square corresponds to the  $16 \times 16$  pixels reference image. In this case the solar limb crosses the sub-aperture images.

pupil is created between TT and DM. A glass parallelepiped (SP) allows shifting the beam before the field stop (FS) of the Shack-Hartmann wave front sensor (SH-WFS). This allows selecting the sub-aperture field of view on which the correction is applied. It is convenient to use the SP also for scanning or for choosing the limb distance in limb tracking mode. The SP movement is controlled manually or by a step motor. The Lens L1 focus the pupil on the micro lens array (MLA). The MLA in combination with the transfer Lens L2 generates  $16 \times 16$  sub-aperture images on the  $256 \times 256$  pixel Dalsa CCD camera.

A copy of the system has been built in laboratory at the *Scuola Universitaria Professionale della Svizzera Italiana* (SUPSI) for tests and characterization.

When operating with the spectrograph, the light reflected by the slit jaw can be observed by a recently installed *slit jaw camera* (SJC) (Baumer TXG06 CCD). A different selection of filters (neutral,  $H_{\alpha}$ , Ca-K) is available. When observing with the Fabry Perot filter system the Spectrograph Slit (SS) block can be shifted away on rails.

Figure 3 shows an example of an image seen by the SHW-FS Dalsa camera during limb tracking. The solar limb crosses the sub-aperture images represented by the small  $8 \times 8$  pixels squares which are used for the wave front measurement. The large square corresponds to the  $16 \times 16$  pixels reference image. The selection of the useful sub-aperture images is done during the calibration procedure with the pinhole, by imposing a selectable minimal and a maximal distance from the center and a minimal intensity. This procedure is driven by the fact that the pupil image contains the shadow of the Gregory mirror and its support bars, which form a cross. Moreover, the sub-aperture image to be used as reference can be freely chosen by the user, so as to avoid that it falls near the support bars shadow. Because of the cross-shaped pupil, for a stable AO operation, it is important that during an observation the derotator corrects for the image and pupil rotation induced by the telescope rotation around the polar axis.

### 3. THE AO CONTROL SYSTEM

The core of the AO system is represented by a general purpose PC with the Linux operating system modified by the RTAI (Real Time Application Interface) add-ons. A low cost acquisition card (Computer Measurements DAQ-PCI1200) is responsible to pilot the driver of the tip-tilt mirror. Two other cards are connected to the driver for the 37 deformable mirror elements.

The camera of the Shack-Hartmann sensor is a Dalsa CA-D6-256. Despite this architecture is basically similar to the one presented by Keller et al.(2003),<sup>7</sup> it offers the following improvements:

- The control part is realized using a hard real-time operating system.
- The calculation and optimization tasks (for example calculation of the reconstruction matrix) are now realized using Scicoslab, which is free available on the WEB.
- Some plots have been added to represent in real-time the effects of the control on the DM and the TT mirrors.
- The software has been reorganized in a modular form allowing a more efficient development.

## **3.1 Software**

### **3.1.1 Software architecture**

The software has been divided into a real-time and a non real-time part:

- The real-time part has been realized as RTAI kernel thread. It is responsible for the sensor, the control algorithm and the actuators.
- The non real-time part handles the menus (HMI: Human Machine Interface) and the representation of the collected data.

In particular, the kernel module contains the driver of the DALSA camera and the procedures to access the registers of the acquisition cards connected to the DM and the TT drivers.

The communication between the hard real-time and the non real-time tasks is implemented using FIFOs, real-time structures realized in RTAI as a circular buffer. A set of 11 FIFOs are used to exchange data between the two applications. The FIFO 0 is used to transmit commands from the HMI to the RT task and has a specific FIFO handler, that allows to use it as a kind of interrupt routine.

A task with high priority is connected to the interrupt of the DALSA Camera and synchronizes the controller part at 1kHz.

The HMI is realized with 3 different windows:

- The input window is used to provide the different commands to the system
- The visualization window with all the information related to the control tasks
- The camera Window realized using Xtoolkit and Xlib with the images from the DALSA camera

### **3.1.2 RTAI**

The PC is running under Linux RTAI, a real-time version of the known Linux operating system (OS). The RTAI extension was created as an environment for implementing low-cost data acquisition and digital controller systems<sup>11,12</sup> and is intended as an open source replacement for other hard real-time OS's such as QNX or VxWorks. This extension adds hard real-time capabilities to Linux, allowing sample frequencies up to several thousands of cycles per second with a jitter of just a few microseconds. Real-time processes can run either in the kernel or in the user area. The low latencies guaranteed by Linux RTAI make it possible to implement controllers for systems with closed-loop bandwidths up to a few hundred Hertz.

One of the authors (RB) is member of the development team of Linux RTAI.

### 3.1.3 Control algorithm

A schematic representation of the current IRSOL adaptive optics controller based on the one developed by Keller et al.(2003)<sup>7</sup> is presented in Figure 4. The incoming light with the distorted wavefront profile  $\phi_{\text{ATM}}$  enters the system and is reflected by the TT and the DM mirrors, which are able to provide a wavefront correction  $\phi_{\text{TT}}$  and  $\phi_{\text{DM}}$  respectively. In this configuration, the TT mirror provides a correcting wavefront contribution for the tip and tilt modes while higher order modes are compensated by the DM. The corrected light with a residual wavefront distortion  $\phi_{\text{RES}}$  is directed to the wavefront sensor  $G$  that delivers the wavefront distortion information at  $N_S$  discretized positions of the pupil.<sup>13</sup> The wavefront slope vector  $\mathbf{p} \in \mathbb{R}^{2N_S \times 1}$ , whose odd and even entries provide slope information about the  $x$  and  $y$  directions respectively, is computed using correlation techniques based on the sum of absolute differences (SAD) algorithm developed by Keller et al. (2003).<sup>7</sup> This algorithm allows a dramatical reduction of the computational time thanks to the use of parallel processor instructions. Each sub-aperture image is compared to a reference image by computing the SAD as a function of displacement of the two images. Then, the entries of the wavefront slope vector  $\mathbf{p}$  for a given sub-aperture will correspond to those coordinates minimizing the SAD between the reference image and the given sub-aperture image. Subsequently, the residual wavefront distortion is reconstructed by the wavefront reconstructor  $R$  by considering the following decomposition into the DM and TT actuator basis

$$\mathbf{p} = \mathbf{D}_{\text{DM}} \cdot \mathbf{m}_{\text{DM}} + \mathbf{D}_{\text{TT}} \cdot \mathbf{m}_{\text{TT}} \quad (1)$$

where  $\mathbf{D}_{\text{DM}} \in \mathbb{R}^{2N_S \times 37}$  and  $\mathbf{D}_{\text{TT}} \in \mathbb{R}^{2N_S \times 2}$  are the DM and TT reconstruction matrices,<sup>13</sup> which can be obtained by a calibration procedure, while  $\mathbf{m}_{\text{DM}} \in \mathbb{R}^{37 \times 1}$  and  $\mathbf{m}_{\text{TT}} \in \mathbb{R}^{2 \times 1}$  are the DM and TT decomposition coefficients. Therefore, the decomposition coefficients  $\mathbf{m}_{\text{DM}}$  and  $\mathbf{m}_{\text{TT}}$  are computed so as to ensure that the DM mirror contributes neither to the tip nor to the tilt modes

$$\mathbf{m}_{\text{DM}} = (\mathbf{D}_{\text{DM}} - \mathbf{A} \cdot \mathbf{D}_{\text{DM}})^+ \cdot (\mathbf{p} - \mathbf{A} \cdot \mathbf{p}) \quad (2)$$

$$\mathbf{m}_{\text{TT}} = \mathbf{D}_{\text{TT}}^+ \cdot \mathbf{A} \cdot \mathbf{p} + \mathbf{D}_{\text{TT}}^+ \cdot \mathbf{A} \cdot \mathbf{D}_{\text{DM}} \cdot \mathbf{m}_{\text{DM}} \quad (3)$$

where we have introduced an averaging matrix  $\mathbf{A} \in \mathbb{R}^{2N_S \times 2N_S}$  whose entries  $\{i, j\}$  are equal to 0 if  $i + j$  is odd and equal to  $1/N_S$  otherwise. The matrix  $\mathbf{A}$  allows computing the average of the slopes along the  $x$  and  $y$  directions of the vector it multiplies. The symbol  $+$  denotes the matrix pseudo inverse operator, which can be computed using the singular value decomposition<sup>14</sup> and appropriate spatial filtering,<sup>13</sup> where only those eigenvectors (mirror orthogonal modes) corresponding to singular values greater than a given threshold are maintained while the remaining discarded. Notice that the second term in Equation 3 corresponds to the DM decoupling contribution. Subsequently, the coefficients  $\mathbf{m}_{\text{DM}}$  and  $\mathbf{m}_{\text{TT}}$  are passed to  $\mathbf{C}_{\text{DM}}$  and  $\mathbf{C}_{\text{TT}}$  that consist of a series of parallel single-input single-output dynamic controllers, which are responsible for stability and closed-loop performance and provide the input voltages for the DM and TT mirrors respectively. The DM and TT temporal controllers are based on standard proportional-integral-derivative (PID) architectures. The control algorithm can also be configured to work in a single axis correction mode ( $x$  or  $y$ ), which is particularly effective for limb tracking.

Control strategies that are able to take full advantage of the spatio-temporal correlation of the wavefront with the objective of minimizing the mean square residual wavefront  $\phi_{\text{RES}}$  error<sup>15, 16</sup> are topic of future investigations.

### 3.1.4 Scicoslab

Scicoslab is a clone of Matlab, and can be freely downloaded from the web<sup>17</sup> and doesn't need to acquire any license to run it.

Scicoslab is used to perform the following tasks:

- Analysis of the DM interactions
- Analysis of the DM modes
- Analysis of the TT interactions
- Building the mirror reconstruction matrices
- Plot of the controller effects on the wavefront correction (see section 3.1.5).

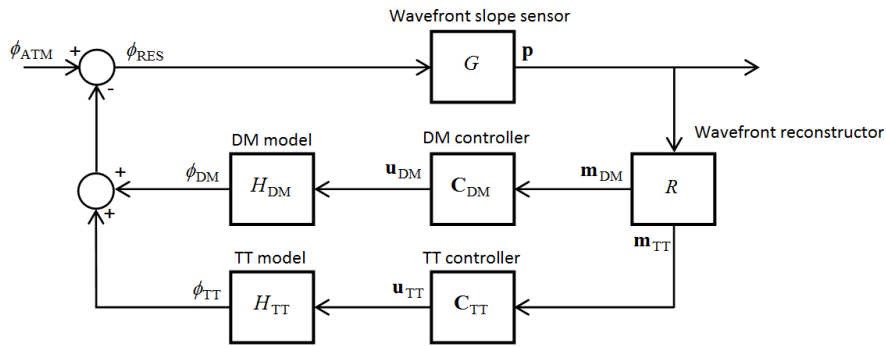


Figure 4. IRSOL Adaptive Optics control architecture

### 3.1.5 Online analysis tools

In order to perform some tests on the system, user have the possibility to plot in run-time some signals, as for instance the applied corrections, the displacements measured by the Shack-Hartmann sensor, the modes of the DM or the reconstructed errors on the DM and TT. This method allows measuring the effect of the AO in run-time as shown in Figure 5.

A separate process running a Scicoslab application is forked for plotting in runtime these signal values.

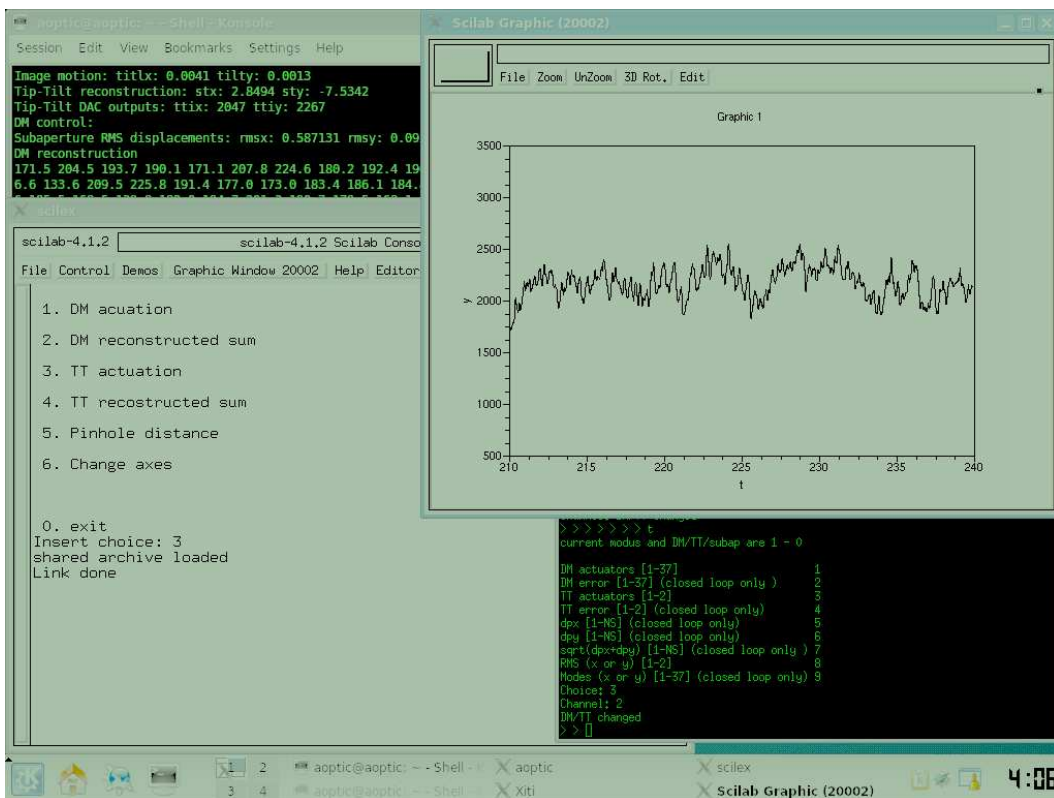


Figure 5. Screenshot taken when operating in closed loop in limb tracking mode. The run-time plot shows the corrections applied to the tip-tilt in the direction perpendicular to the limb in arbitrary internal units.

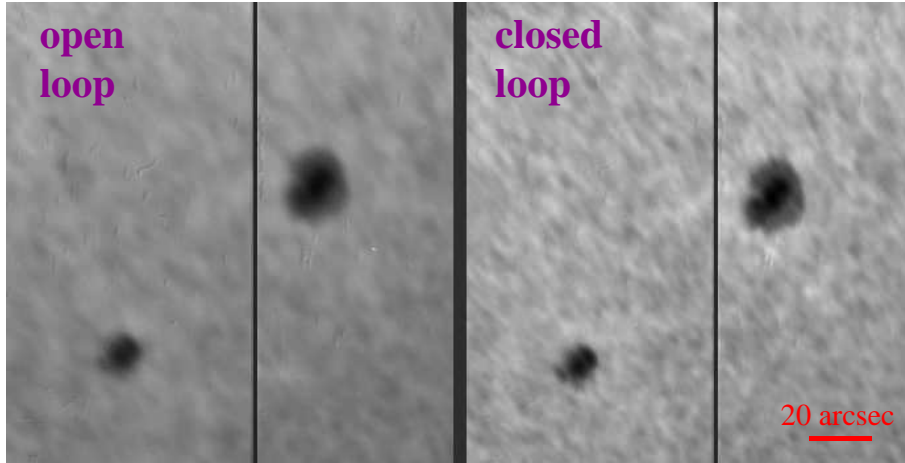


Figure 6. Sunspot group observed in open and closed loop by the slit-jaw camera. Images obtained averaging 60 frames recorded during 30 seconds.

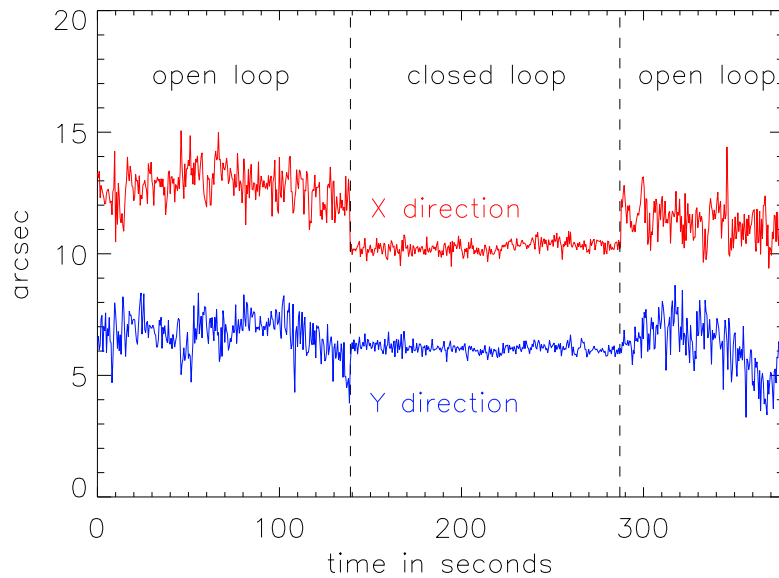


Figure 7. Movement of the center of gravity of the largest sunspot shown in Fig. 6

#### 4. PERFORMANCE

In Figure 6 we show an example of observations of a small sunspot group with the AO recorded with average seeing conditions in open and in closed loop. The images have been obtained averaging 60 frames of 30 ms exposure each, recorded with the slit-jaw camera (SJC) at a frame rate of 2Hz. The oscillation of the center of gravity of the largest spot on the right is plotted on Fig. 7. One can see a clear improvement in the image stability when the AO is in closed loop.

Also the operation in limb tracking mode (on the axis perpendicular to the limb) works in a satisfactory way. Fig. 8 shows a comparison between the limb oscillations observed in closed and in open loop. The limb position has been determined by an automatic procedure that finds the intensity inflection point for each pixel row on the slit jaw image and then fits a circle with the given solar radius. With the limb tracking mode we could also obtain first scientific observations.<sup>18</sup>

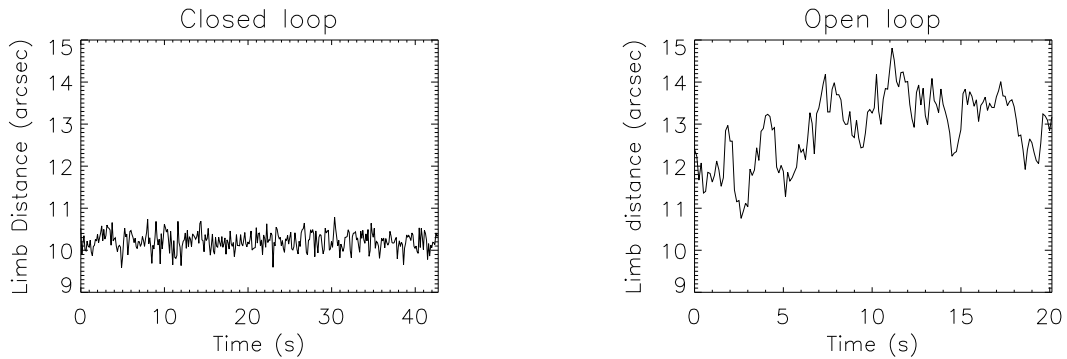


Figure 8. The oscillations of the distance between limb and spectrograph slit in closed and open loop observed during a day of rather poor seeing conditions. The AO applies here the corrections only on the horizontal axis, which is perpendicular to the limb

A drawback of the observations with the AO is the decrease of the overall transmission efficiency, because of the beam splitter and the several additional mirrors present in the light path. However we should notice that this is largely compensated by other recent instrumental improvements. In particular the recent successful installation of cylindrical micro-lenses on the ZIMPOL CCD<sup>3</sup> increased the efficiency by about a factor 4 (even a factor 6 in the near UV). In addition with the new generation of cameras ZIMPOL3 we could lower the time overhead.<sup>3</sup>

## 5. CONCLUSION AND OUTLOOK

We could successfully test our AO system at IRSOL in limb tracking mode and on sunspots. We could also start using it in a satisfactory way for scientific observations. Our AO shows that the concept of the system, that has been originally developed by Keller et al. (2003)<sup>7</sup> for the infrared AO at the McMath-Pierce telescope, works as well in the optical range. New features that were added to the IRSOL AO, with respect to the original Keller’s design, include the installation on a Real Time OS (RTAI), the inclusion of online analysis tools, and a reorganization of the software in a modular form which allows a more efficient development. In future we plan to further work on the optimization of the system, taking advantage also of the presence of a copy of the system in the laboratory.

## ACKNOWLEDGMENTS

This project has been supported by Swiss National Science Foundation grant 200020-117821. IRSOL observatory is financed by Canton Ticino, ETHZ and City of Locarno together with the municipalities affiliated to CISL. Leopoldo Rossini would like to thank the *Fondazione Rudolf Chaudoire* for financially supporting his work during this AO project.

The authors are in debt with Christoph Keller for clarifying discussions and important advice.

## REFERENCES

- [1] Bianda, M., Ramelli, R., and Gisler, D., “Observing the Second Solar Spectrum at IRSOL,” in [*Solar Polarization 5: In Honor of Jan Stenflo*], S. V. Berdyugina, K. N. Nagendra, & R. Ramelli, ed., *Astronomical Society of the Pacific Conference Series* **405**, 17–21 (June 2009).
- [2] Gandorfer, A. M., Steiner, P., Povel, H. P., Aebersold, F., Egger, U., Feller, A., Gisler, D., Hagenbuch, S., and Stenflo, J. O., “Solar polarimetry in the near UV with the Zurich Imaging Polarimeter ZIMPOL II,” *Astron. Astrophys.* **422**, 703–708 (Aug. 2004).
- [3] Ramelli, R., Balemi, S., Bianda, M., Defilippis, I., Gamma, L., Hagenbuch, S., Rogantini, M., Steiner, P., and Stenflo, J. O., “ZIMPOL-3: a powerful solar polarimeter,” in [*SPIE Conference Series*], **7735**, 238 (2010).

- [4] Hanle, W., “Über magnetische Beeinflussung der Polarisation der Resonanzfluoreszenz,” *Z. Phys.* **30**, 93–105 (1924).
- [5] Berdyugina, S. V., Nagendra, K. N., and Ramelli, R., eds., [*Solar Polarization 5: In Honor of Jan Stenflo*], *Astronomical Society of the Pacific Conference Series* **405** (June 2009).
- [6] Stenflo, J. O., “The Hanle effect and the diagnostics of turbulent magnetic fields in the solar atmosphere,” *Solar Phys.* **80**, 209–226 (Oct. 1982).
- [7] Keller, C. U., Plymate, C., and Ammons, S. M., “Low-cost solar adaptive optics in the infrared,” in [*SPIE Conference Series*], S. L. Keil & S. V. Avakyan, ed., **4853**, 351–359 (Feb. 2003).
- [8] Feller, A., Bianda, M., and Stenflo, J. O., “Imaging polarimetry with a tunable narrow-band filter,” in [*Modern solar facilities - advanced solar science*], F. Kneer, K. G. Puschmann, & A. D. Wittmann, ed., 63–66 (2007).
- [9] Feller, A., *Instrument Systems for Imaging Spectro-Polarimetry*, PhD thesis, ETH-Zurich (2007).
- [10] Kleint, L., Feller, A., and Bianda, M., “Combination of two Fabry-Perot etalons and a grating spectrograph for imaging polarimetry of the Sun,” *SPIE Conference Series* **7014**, 701414 (Aug. 2008).
- [11] Beal, D., Bianchi, E., Dozio, L., Hughes, S., Mantegazza, P., and Papacharalambous, S., “RTAI: real time applications interface,” *Linux Journal* **14**, 185–192 (2000).
- [12] Bianchi, E. and Dozio, L., “Some experience in fast hard real-time control in user space with RTAI-LXRT,” in [*Real Time Linux Workshop*], (2000).
- [13] Tyson, R. K., [*Introduction of adaptive optics*], SPIE Press, Bellingham, Washington (2000).
- [14] Golub, G. H. and Van Loan, C. F., [*Matrix Computations*], The Johns Hopkins University Press, 3rd ed. (1996).
- [15] Dessenne, C., *Commande modale et prdictive en optique adaptive*, PhD thesis, Ecole Doctorale d’Astronomie d’Ile de France, France (1998). ONERA Publication FR ISSN 0078-3780.
- [16] Hinnen, K., Verhaegen, M., and Doelman, N., “Exploiting the spatiotemporal correlation in adaptive optics using data-driven h2-optimal control,” *J. Opt. Soc. Am.* **24**, 1714–1725 (2007).
- [17] Scicoslab, “A free scientific software package.” [www.scicoslab.org](http://www.scicoslab.org).
- [18] Ramelli, R., Trujillo Bueno, J., Bianda, M., and Asensio Ramos, A., “Measurement of the magnetic field in prominences and spicules through spectropolarimetry of the Helium D3 multiplet,” in [*Solar Polarization 6*], *Astronomical Society of the Pacific Conference Series*, in press (2010).